Lattice Boltzmann simulations of droplet breakup in confined and time-dependent flows

Felix Milan [●],[1,2,*] Luca Biferale,[1,†] Mauro Sbragaglia,[1,‡] and Federico Toschi [●][2,3,4,§]

[1]*Department of Physics and INFN, University of Rome "Tor Vergata", Via della Ricerca Scientifica 1, 00133 Rome, Italy*
[2]*Department of Applied Physics, Eindhoven University of Technology, Eindhoven 5600 MB, The Netherlands*
[3]*Department of Mathematics and Computer Science, Eindhoven University of Technology, Eindhoven 5600 MB, The Netherlands*
[4]*CNR-IAC, Via dei Taurini 19, 00185 Rome, Italy*

We study droplet dynamics and breakup in generic time-dependent flows via a multi-component lattice Boltzmann algorithm, with emphasis on flow startup conditions. We first study droplet breakup in a confined oscillatory shear flow via two different protocols. In one setup, we start from an initially spherical droplet and turn on the flow abruptly ("shock method"); in the other protocol, we start from an initially spherical droplet as well, but we progressively increase the amplitude of the flow, by allowing the droplet to relax to the steady state for each increase in amplitude, before increasing the flow amplitude again ("relaxation method"). The two protocols are shown to produce substantially different breakup scenarios. The mismatch between these two protocols is also studied for variations in the flow topology, the degree of confinement, and the inertia of the fluid. All results point to the fact that under extreme conditions of confinement the relaxation protocols can drive the droplets into metastable states, which break only for very intense flow amplitudes, but their stability is prone to external perturbations, such as an oscillatory driving force.

I. INTRODUCTION

Fluid dynamics phenomena, involving droplet dynamics, deformation, and breakup, are prominent in the field of microfluidics and even in general complex flows at larger scales. Beyond the practical importance in a variety of concrete applications [1–4], they are also relevant from the theoretical point of view, due to the complexity of the physics involved [5–9]. Droplet deformation is characterized via the capillary number,

$$\mathrm{Ca} = \frac{\eta_s R G}{\sigma}, \tag{1}$$

where η_s is the dynamic viscosity of the solvent, R the radius of the initially undeformed spherical droplet, σ the surface tension, and G the shear rate intensity [9,10]. The value of Ca at breakup is denoted by $\mathrm{Ca_{cr}}$, the critical capillary number. A lot of attention has been dedicated to droplet deformation and breakup in stationary flows [5,11,12] and, in particular, the effect of the degree

---

*felix.milan@roma2.infn.it
†biferale@roma2.infn.it
‡sbragaglia@roma2.infn.it
§f.toschi@tue.nl

of confinement on the flow dynamics [13–15]. The degree of confinement is parametrized by the ratio $\alpha = 2R/L$, where L denotes the shear wall separation. Confinement is frequently encountered in experimental setups of droplet dynamics in simple shear flows [13–24] and can be enhanced by changing α. There are some theoretical models which were developed to capture the experimental phenomenology of confined droplet dynamics, analytical models [25,26], which extended the theory by Taylor [9,27], and phenomenological models [28–30]. The validity of the analytcial models were verfied in Ref. [31] and the phenomenological models in [32]. Of particular interest are the results in Ref. [14], which show that, for nonvanishing α breakup differs substantially from the unconfined shear case both qualitatively and quantitatively for all viscosity ratios $\chi = \eta_d/\eta_s$, where $\eta_{d,s}$ is the dynamic viscosity of the droplet (d) or solvent (s) phase. Additionally, the dependency of the critical capillary number $\mathrm{Ca_{cr}}$ on the droplet's inertia is a central area of interest [7,33–53], with the degree of inertia being given by the Reynolds number,

$$\mathrm{Re} = \frac{GR^2}{\nu_S}, \tag{2}$$

where ν_S is the kinematic viscosity of the solvent. Furthermore, breakup is influenced by the startup conditions, as demonstrated in experimental and theoretical studies [54–58]. This phenomenon is rather subtle and can have different effects depending on the protocol in use. The dependency on the rate of increase of the shear rate G was confirmed by Ref. [58] via supporting calculations based on the model by Taylor [9]. A theoretical model developed by Hinch *et al.* [56] shows that stable droplet equilibria below the critical capillary number $\mathrm{Ca_{cr}}$ breakup are only possible for a sufficiently low increase in G. Furthermore, Renardy [57] has shown that although these stable equilibria require a slow increase in the shear rate G they are unique and do not depend on the rate of change of G. We stress that even though the effect of startup conditions on breakup has been investigated [54–58], the role of confinement with varying startup conditions on droplet dynamics and breakup is not clear. Moreover, it is unclear how breakup is affected, if the flows are time-dependent [59–63]. The aim of the present paper is to take a step further in this direction. With the use of numerical simulations we show that at capillary numbers close to breakup, confinement allows for the existence of a metastable flow configuration next to the solution of the Stokes equation found in Ref. [57]. This metastable state is prone to perturbations and collapses to the Stokes solution, if we have a time-dependent flow with a sufficiently large shear frequency. It should be stressed that this result is unique to the case of a confined droplet in an oscillatory shear, as this metastable configuration is not present neither for an unconfined droplet in an oscillatory shear flow nor in the case of an oscillatory elongational flow. Our studies can be seen as an extension to Refs. [50,57], where the influence of inertia on droplet breakup was studied, whereas we deal with time-dependent cases, where the temporal rate of change of the shear intensity is comparable to the droplet relaxation time,

$$t_d = \frac{\eta_d R}{\sigma}. \tag{3}$$

This work is a followup study of Ref. [62], where stable time-dependent droplet dynamics was investigated via a multicomponent lattice Boltzmann scheme and a phenomenological model [28,29]. It was found that droplet deformation depended strongly on an external timescale, the oscillation frequency of an oscillatory shear flow, for a confined droplet. For relatively large oscillation periods close to the value of t_d the droplet is hardly deformed by the solvent shear flow, which was described as the "transparency effect" in Ref. [62]. The findings in Ref. [62] have been validated by comparing the lattice Boltzmann results to the results obtained via a phenomenological droplet deformation model, the Maffettone-Minale model [28,29].

This paper is organized as follows: Sec. II gives a brief overview on the lattice Boltzmann algorithms and models in use. In Sec. III, we outline the general details of droplet breakup with an emphasis on confined systems and simple shear flows. In Sec. IV, we investigate breakup in a time-dependent (oscillatory) shear flow under strong confinement. A mismatch between two protocols, involving different startup conditions of the flow, leads us to investigate breakup conditions under

the influence of inertia (Sec. V) and the effect of confinement (Sec. VI). Moreover, we check whether the protocol mismatch depends on the flow topology (Sec. VII).

II. LATTICE BOLTZMANN ALGORITHMS AND METHODS

We use lattice Boltzmann simulations [64,65] to study droplet breakup in confined and time-dependent shear and elongational flows. The lattice Boltzmann method (LBM) has been extensively used in the field of microfluidics, including extensions to accommodate nonideal effects [66], coupling with polymer micromechanics [67] and thermal fluctuations [68,69]. LBM has also been used widely for the modeling of droplet breakup behavior [41,44,70–77]. To model multicomponent systems with the lattice Boltzmann model (LBM), we need to account for interfacial forces between different fluid components. This can be achieved with the Shan-Chen multicomponent model (SCMC) [78,79], a diffuse interface model in the framework of the LBM. The hydrodynamical quantities, mass and momentum densities, can then be described as

$$\rho(\mathbf{x}, t) = \sum_{\sigma} \sum_{i} g_i^{\sigma}(\mathbf{x}, t), \quad \rho(\mathbf{x}, t)\mathbf{u}(\mathbf{x}, t) = \sum_{\sigma} \sum_{i} g_i^{\sigma}(\mathbf{x}, t)\mathbf{c}_i, \tag{4}$$

where $g_i^{\sigma}(\mathbf{x}, t)$ denotes the populations in the LBM model for the fluid component σ and $\mathbf{c}_i$ are the lattice velocities. For example, for a two-component system with species A and B the index σ can take the values $\sigma = A$ and $\sigma = B$. The interaction at the fluid-fluid interface [80,81] is given by

$$\mathbf{F}^{\sigma}(\mathbf{x}, t) = -\rho_{\sigma}(\mathbf{x}, t) \sum_{\sigma' \neq \sigma} \sum_{i=1}^{N} \mathcal{G}_{\sigma,\sigma'} w_i \rho_{\sigma'}(\mathbf{x}, \mathbf{t} + \mathbf{c}_i)\mathbf{c}_i, \tag{5}$$

where $\rho_{\sigma}(\mathbf{x}, t)$ is the density field of the fluid component denoted by σ. $\mathcal{G}_{\sigma,\sigma'}$ is a coupling constant for the two phases σ and σ' at position $\mathbf{x}$ and w_i are the lattice isotropy weights. We use the same open flow boundary conditions as outlined in Ref. [62]. To use arbitrary boundary values of the density $\rho(\mathbf{x}, t)$ and velocity $\mathbf{u}(\mathbf{x}, t)$ fields of the solvent fluid we use ghost populations (or halos), which store the equilibrium distribution functions g_i^{eq} of the boundary density and velocity fields. The equilibrium distribution functions g_i^{eq} are given by

$$g_i^{\text{eq}}(\mathbf{x}, t) = \rho_b(\mathbf{x}, t)w_i\left(1 + 3\,\mathbf{c}_i \cdot \mathbf{u} + \tfrac{9}{2}(\mathbf{c}_i \cdot \mathbf{u})^2 - \tfrac{3}{2}\mathbf{u}^2\right), \tag{6}$$

with w_i being the lattice weights for the set of lattice vectors $\mathbf{c}_i$ and $\rho_b(\mathbf{x}, t)$ the density field at the simulations domain boundary. Thus, the ghost distributions update the boundary nodes during the LBM streaming step and effectively simulate an open flow boundary given by the chosen density $\rho_b(\mathbf{x}, t)$ and velocity $\mathbf{u}(\mathbf{x}, t)$ fields of the outer fluid [62]. The streaming and collision steps are given by the lattice Boltzmann equation:

$$g_i(\mathbf{x} + \mathbf{c}_i\Delta t, t + \Delta t) - g_i(\mathbf{x}, t) = \Omega(\{g_i(\mathbf{x}, t)\}), \tag{7}$$

where $\Omega(\{g_i(\mathbf{x}, t)\})$ is the collision operator depending on the whole (local) set of lattice populations and Δt is the simulation time step. For MRT (multirelaxation timescale) the collision operator is linear and contains several relaxation times linked to its relaxation modes (depending on the lattice stencil) [82]. One relaxation time τ is directly linked to the kinematic viscosity ν in the system

$$\nu = \tfrac{1}{3}\left(\tau - \tfrac{1}{2}\right), \tag{8}$$

which is one of the primary links between the LBM scheme and hydrodynamics [64,65]. The boundary scheme described here is not strictly mass conserving, so we correct the local population mass densities to cure mass conservation [83–85]. This is not the case in unconfined system, where we can accept small mass fluctuations of both droplet and solvent, but have to reinject mass into the droplet [86].

III. SIMULATION SETUP AND DEFINITIONS

In this section we define what we mean when we speak of droplet breakup and characterize the simulation setups. We deal with both a confined droplet in a simple shear flow and an unconfined droplet in a uniaxial extensional (elongational) flow. The velocity gradient matrix for both shear and elongational flows is given by

$$\nabla \mathbf{v} = \frac{G}{2} \begin{pmatrix} \beta & 0 & 2(1-\beta) \\ 0 & \beta & 0 \\ 0 & 0 & -2\beta \end{pmatrix}, \tag{9}$$

where $\|\nabla \mathbf{v}\| = G$ and β is a parameter characterizing the flow type. The shear flow setup is equivalent to the one used in Ref. [62] with $\beta = 0$ in Eq. (9) except that the flow is unconfined and elongational with an oscillatory velocity gradient amplitude $G(t)$ given by Eq. (9) with $\beta = 1$. Droplet deformation can be characterized by the capillary number Ca. In the case of a shear flow including confinement the shear rate is given by

$$G = \frac{2u_0}{L_z}, \tag{10}$$

with L_z being the channel width responsible for the droplet confinement and u_0 being the maximum wall velocity amplitude. This definition may also be extended to time-dependent shear flows [62],

$$G(t) = \frac{2u(t)}{L_z}, \tag{11}$$

In accordance with Ref. [14], we define the critical capillary number Ca_{cr} as the value of Ca for which an initially spherical droplet breaks up, which is achieved by a sudden increase in the shear rate amplitude G. We refer to this breakup protocol as the *shock method*. In addition we can gradually increase the shear rate G starting from a value for which the droplet is only marginally deformed [56–58]. A fixed increase ΔG [or Δu_0 in the case of Eq. (11)] is equivalent to a fixed increment rate ΔCa for the capillary number. This way the droplet and the solvent flow are given more time to relax to their respective equilibrium distributions at specific Ca. We call this protocol the *Relaxation method*. It should be stressed that breakup in the relaxation method has a small dependency on ΔCa. If ΔCa is very large, e.g., $\Delta Ca \sim Ca_{cr}$, then the value for Ca_{cr} will be the same as the one obtained through the shock method. Thus, the ΔCa has to be chosen sufficiently small enough for the relaxation method to work. Essentially, the relaxation method captures the deformation history of the droplet before breakup with an accuracy given by ΔCa contrary to the shock method. The relaxation method is especially important for droplet dynamics in palatially evolving shear flows in the case of a smoothly varying local shear both spatially and temporally. A variation of the relaxation method for time-dependent oscillatory flows, i.e., where the shear amplitude $G(t) = G_0 \cos(\omega t)$, is to consider the flow and droplet configuration at a capillary number Ca close to Ca_{cr} and then to increase the oscillatory shear frequency $\omega_f = \omega/(2\pi)$ until breakup, starting from the stationary case of $\omega_f = 0$. As in Ref. [62] we use a dimensionless frequency $\omega_f t_d$ in our discussion, where t_d is the droplet relaxation time defined in Eq. (3). In the presence of a flow with nonzero frequency $\omega_f t_d$, we focus on Ca_{max}, which denotes the maximum value of the time-dependent capillary number $Ca(t)$ over one oscillatory cycle [62]. An instance of droplet breakup in an oscillatory simple shear flow is depicted in Fig. 1. The droplet is oscillating between two maximally elongated states for $Ca < Ca_{cr}$ and breaks up during the flow build up for $Ca > Ca_{cr}$ in the case of the shock method. The droplet elongation is characterized by the droplet length $L(t)$, which is defined as the longest axis of the elongated droplet, and L_{cr} denotes the droplet length in the critical case $Ca \geqslant Ca_{cr}$. The time evolution of $L(t)$ is also shown for the two cases $Ca < Ca_{cr}$ and $Ca > Ca_{cr}$ in Fig. 1, which shows that breakup occurs at around $t = 17\,000$ lbu with lbu denoting lattice Boltzmann Units. In all simulations in this article the viscous ratio $\chi \equiv 1$ and the density ratio $\rho_d/\rho_s \equiv 1$. If not explicitly stated otherwise, then the confinement ratio for simple shear flows
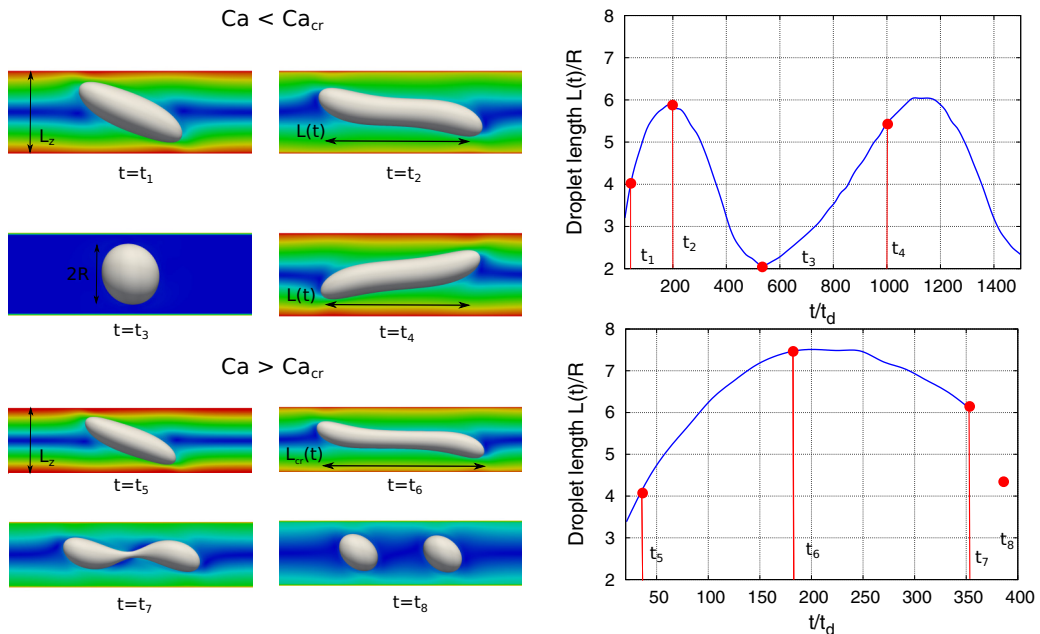
FIG. 1. Snapshots of a droplet in a confined oscillatory shear flow with a nondimensionalized oscillation frequency $\omega_f t_d$. Snapshots of the droplet in the velocity field are shown for Ca $<$ Ca$_{cr}$ and Ca $>$ Ca$_{cr}$. The plots on the right panel show the time evolution of the normalized droplet length $L(t)/R$. The degree of confinement of the system is given by $\alpha = 2R/L_z$, where R is the droplet radius of the undeformed droplet and L_z is the wall separation.

$\alpha \equiv 2R/L_z$, where R is the radius of the spherical undeformed droplet and L_z the channel width, is set to $\alpha = 0.75$.

IV. DROPLET BREAKUP IN AN OSCILLATORY SHEAR FLOW

Similar to Ref. [62] we consider a droplet in a confined oscillatory simple shear flow, see Fig. 2. The setup is shown in Fig. 1 with a confinement ratio $\alpha = 0.75$ and a time-dependent shear rate $G(t) = 2u_0/L_z \cos(2\pi\omega_f t)$, where ω_f is the frequency of the outer oscillatory flow [59–63]. Our main focus is the dependency of Ca$_{cr}$ on the normalized shear frequency $\omega_f t_d$ of the oscillatory outer flow. Droplet dynamics in oscillating flows may feature a so called transparency effect [62], which states that the droplet is hardly deformed if $\omega_f t_d \sim 0.1$, i.e., the timescale of the oscillating shear flow $1/\omega_f$ is of the similar order as the droplet relaxation timescale t_d. The droplet dynamics are hardly influenced by the shear frequency for $\omega_f t_d \sim 10^{-4}$ and the transparency effect is noticeable for $\omega_f t_d \sim 10^{-2}$ and higher frequencies, which leads to a sudden increase in the critical capillary number. To stay in tune with experimental results [14,15,22,23], we limit the range of the critical capillary number close to Ca$_{cr} \sim 1.0$. In Fig. 3 we can see that the droplet breakup behavior is significantly different for our two LBM simulation protocols, the shock and relaxation method. The shock method implies that droplet breakup is independent of the oscillatory shear frequency $\omega_f t_d$, significant changes in Ca$_{cr}$ only occur close to the transparency effect region at high frequencies ($\omega_f t_d \sim 10^{-2}$). The relaxation method is of a different nature: first of all Ca$_{cr}$ in the low-frequency region ($\omega_f t_d \sim 10^{-4}$) is larger than the values obtained with shock method (see also Sec. VI). Moreover, for intermediate frequencies $\omega_f t_d \sim 5 \times 10^{-3}$ we observe that breakup occurs at a significantly smaller Ca$_{cr}$ than in the low-frequency range and is now of a comparable value to Ca$_{cr}$ obtained via the shock method. The mismatch between the two protocols in the low-frequency
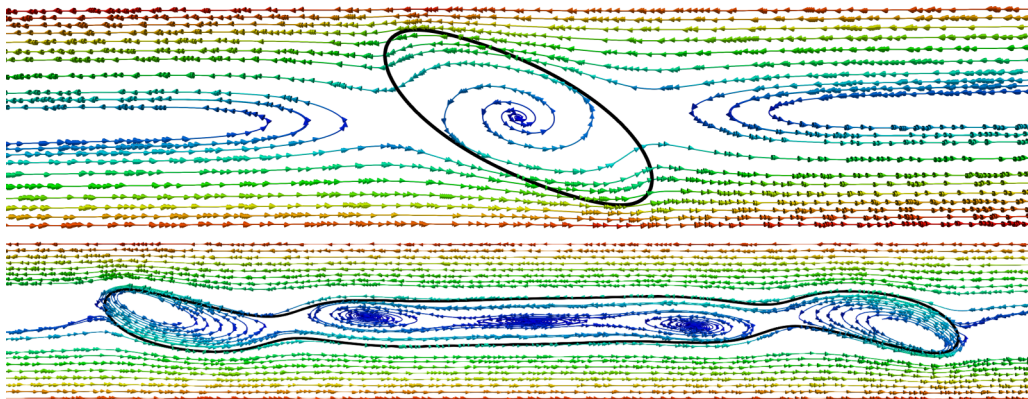
FIG. 2. Planar cut of a droplet in a shear flow, featuring an ellipsoidally deformed droplet and large droplet deformation before breakup. The droplet contours are shown in black and the velocity field is visualized by streamlines coloured according to the velocity magnitude.

regime in Fig. 3 is in disagreement with previous studies of startup conditions of droplet breakup in confined simple shear flows [14,57]. However, the shock method produces results in accordance with the literature [14], as the dashed line in Fig. 3 indicates. It should also be noted, that the destabilization of the "relaxation branch" is rather sudden and takes place at very small $\omega_f t_d$. This suggests that the protocol mismatch is due to metastable solution (relaxation method) existing next to a stable solution (shock method) in the low-frequency range $\omega_f t_d \leqslant 0.02$. The protocol mismatch seems rather puzzling: according to Renardy [57] the solution should be unique. However, our setup differs in a few points from the one in Renardy [57]. First of all, the droplet is strongly confined ($\alpha = 0.75$) in our setup (see Fig. 1), which could have a strong effect on the values Ca_{cr} for varying startup conditions. Moreover, inertia might stabilise the droplet in the case of the relaxation method.
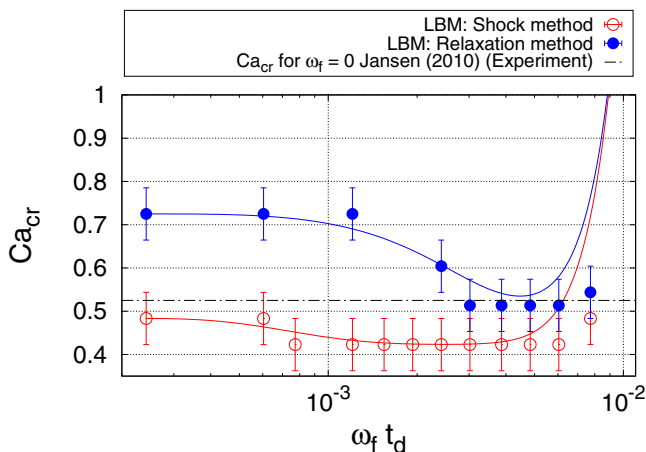

FIG. 3. Critical capillary number Ca_{cr} at varying frequencies $\omega_f t_d$. There is a mismatch between the predictions of the two breakup protocols. Whereas droplet breakup is largely independent in the case of the *shock method*, except for the asymptotic behavior in the high frequency region, the *relaxation method* in the low-frequency limit predicts a higher Ca_{cr} than the ones of the shock method. This mismatch is investigated in the article. The error bars are estimated via steps in the critical capillary number ΔCa. Both curves are interpolated via bezier curves.
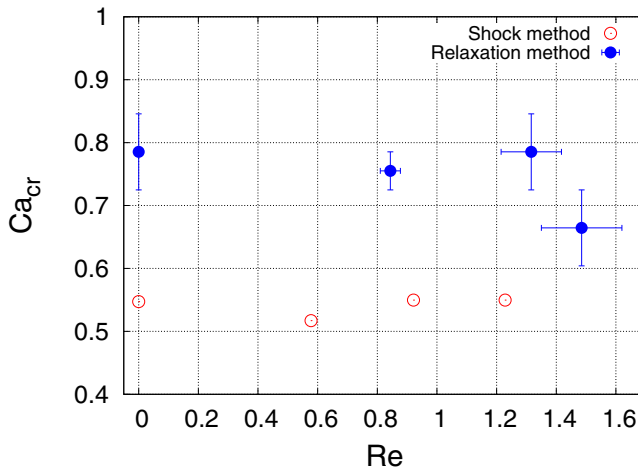
FIG. 4. Ca_{cr} vs. Reynolds number Re. The mismatch between the shock and relaxation breakup protocols does not depend on inertia. This is especially clear in the case of the Stokes solution, for which Re = 0. The error bars are estimated via steps in the critical capillary $\triangle Ca$ and Reynolds number $\triangle Re$.

Therefore, the protocol mismatch might disappear in the Stokes limit. In addition, one may also wonder what is the effect of flow topology, as an inherently different flow field might lead to a similar protocol mismatch. Given these considerations, in the following sections, we will investigate the cause of the mismatch by considering both inertial effects, as is the case in Ref. [57] (see Sec. V) and the importance of confinement in stationary shear flows (see Sec. VI). Regarding the importance of flow topology, we investigate time-dependent breakup in an elongational flow in Sec. VII.

V. INERTIAL EFFECTS

In Ref. [57] it is shown that the solution of the Stokes equation in confined simple shear flows is unique and does not depend on neither the initial conditions of the droplet nor the solvent flow configuration. Thus, one might think that the protocol mismatch might be due to inertial effects and would disappear, if we were close to the time-dependent Stokes limit of Re $\equiv$ 0. Interestingly, the LBM formalism allows us to directly set Re = 0, as we can eliminate the nonlinear terms in the equilibrium distribution functions in the LBM algorithm, Eq. (6), which leads us to a modified Eq. (12), accounting only for the linear terms in the velocity field $\mathbf{u}(\mathbf{x}, t)$. It should be remarked that only the nonlinearites of the Navier-Stokes equation are removed in this way, since the inertia embedded in the time derivative of the velocity field $\mathbf{u}(\mathbf{x}, t)$ does not disappear and may still play a role during the non steady breakup process. Inertial effects tend to stabilise the droplet [54,55] for low Re < 1, whereas $Ca_{cr} \sim 1/Re$ for large Re > 10 [50]. This suggests that the stabilization effect of low Re are responsible for the protocol mismatch, which consequently should disappear in the Stokes limit Re = 0. We investigate the dependency of Ca_{cr} on Re, as shown in Fig. 4. For the case Re = 0 we use only the linear terms of the equilibrium distribution functions given by

$$g_i^{\text{eq,lin}}(\mathbf{x}, t) = \rho_b(\mathbf{x}, t) w_i (1 + 3\, \mathbf{c}_i \cdot \mathbf{u}). \tag{12}$$

The simulations are carried out for a stationary shear flow, with the setup described in Fig. 1. We can see that the mismatch between the breakup protocols, does not depend on inertia and is even present in the Stokes limit of Re = 0. We conclude that the mismatch between the two breakup protocols is not influenced by any stabilization effects of inertia [54,55] for the given range of Reynolds numbers Re $\sim$ 0.0, . . . , 1.5.
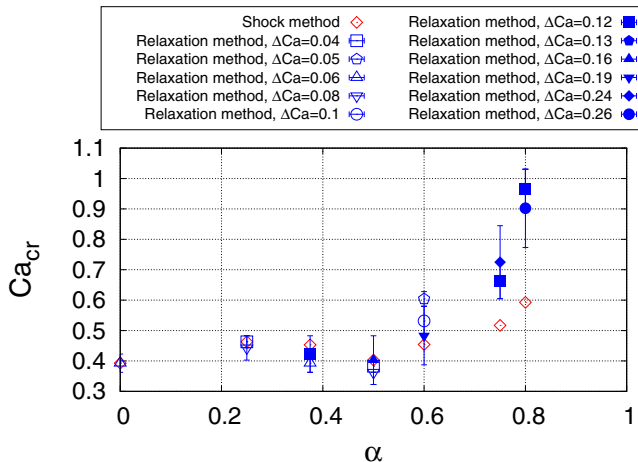
FIG. 5. Critical capillary number Ca_{cr} for different confinement ratios $\alpha = 2R/L_z$. We compare the values obtained by the LB simulations with the shock method and the ones obtained by the relaxation method. Since the relaxation method is dependent on the startup conditions of the outer flow and the droplet, we provide a range of different increments ΔCa, where smaller ΔCa denote a slower and flow build up and vice versa. The error bars are estimated via steps in the critical capillary number ΔCa. For each simulation run of the relaxation method with a given Ca we gave the droplet a sufficiently long time to relax to its stationary state.

VI. CONFINEMENT EFFECTS

We now focus on both confinement and startup conditions in the shear rate amplitude G for droplet breakup in a stationary shear flow. The setup is once again the one in Fig. 1, a confined droplet in a stationary ($\omega_f t_d = 0$) shear flow, but now we vary the confinement ratio α and, in the case of the relaxation method, the rate of change of the shear amplitude G, resulting in increments of the capillary number ΔCa. Our results are summarized in Fig. 5. We can see, as was shown in Ref. [57], that the critical capillary number Ca_{cr} is independent of the startup conditions for low confinement ratios ($\alpha \leqslant 0.5$), as both the shock method and the relaxation method yield the same results with respect to the simulation errors. However, if the droplet is strongly confined ($\alpha \geqslant 0.6$), then the two methods yield very different results, with the Ca_{cr} predicted by the relaxation method being substantially larger than the one predicted by the shock method. It should be noted, that Ca_{cr} is independent of ΔCa, given that ΔCa is small enough, which can be seen from Fig. 5, where the values of Ca_{cr} overlap in respect to their error ranges for different ΔCa and the same α. Figure 6 shows the length of the elongated droplet as a function of the LB simulation time for the different shear startup methods: we can see that for the shock method droplet breakup occurs soon after the maximal elongation, whereas for the relaxation the droplet experiences a sequence of maximal extensions and subsequent retractions after breaking up for a given Ca_{cr} at its critical length $L_{cr}(t)$. We conclude that both a slow startup of the outer flow (relaxation method) and a strong confinement of the droplet ($\alpha \geqslant 0.6$) are necessary for the mismatch reported in Fig. 3 in the low-frequency limit. The eventual collapse of the relaxation method solution on to the one found by the shock method suggests, that the relaxation method branch in the low-frequency limit in Fig. 3 is a metastable state, explaining the high susceptibility to small perturbations and the collapses to the configuration obtained by the shock method for intermediate oscillatory frequencies $\omega_f t_d$.

VII. FLOW TOPOLOGY

We now investigate the protocol mismatch in terms of the flow topology. Instead of an oscillatory shear flow, we consider breakup in an elongational (or uniaxial extensional) flow; see Fig. 7. This flow is by its very nature unconfined, so we would expect to not see a mismatch, as is the case
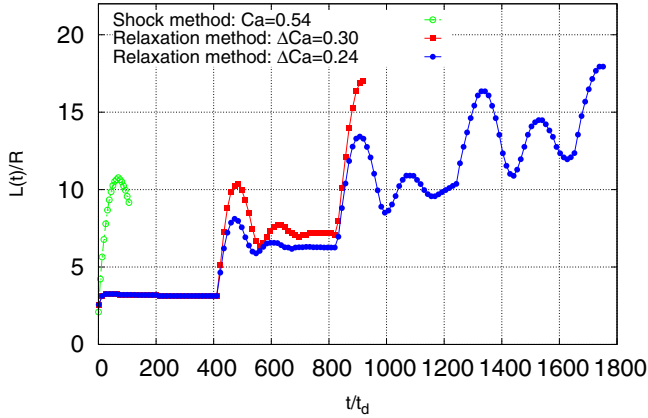
FIG. 6. Normalized droplet major axis $L(t)/R$ against simulation time t given in units of the droplet relaxation time t_d. The droplet breaks up shortly after its maximum elongation for the shock method. Breakup in the relaxation method is dependent on the shear rate and thus capillary number increase: (a) for a rate with increment $\Delta\text{Ca} = 0.30$ the droplet relaxes after reaching its maximum elongation for the first time to breakup at a longer length at a higher Ca_{cr} later on; (b) for a smaller capillary number increase $\Delta\text{Ca} = 0.24$ the droplet length at Ca_{cr} increases even further and the $L(t)$ contains more full extensions and subsequent retractions.

for $\alpha = 0$ in the case of the confined shear flow; see Sec. VI. The results are shown in Fig. 8. Interestingly, a mismatch between the two droplet protocols is absent and the predictions agree well with each other in terms of their respective errors. This shows that strong confinement ($\alpha \geqslant 0.75$) is necessary for the existence of the protcol mismatch shown in Fig. 3. Moreover, Fig. 8 shows that droplet breakup in an oscillatory elongational flow is frequency dependent, with an exponential dependence between the oscillation frequency $\omega_f t_d$ and the critical capillary number Ca_{cr}. The low-frequency limit matches the stationary flow predictions of Ref. [39].
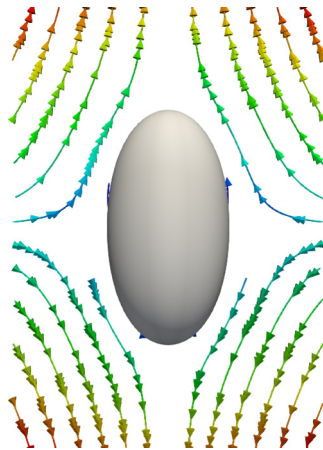

FIG. 7. The flow layout of a droplet in an elongational (uniaxial extensional) flow. The image is a planar cut, with the flow being rotational symmetric around the elongated droplet axis in the image. The streamlines are coloured according to the velocity magnitude.
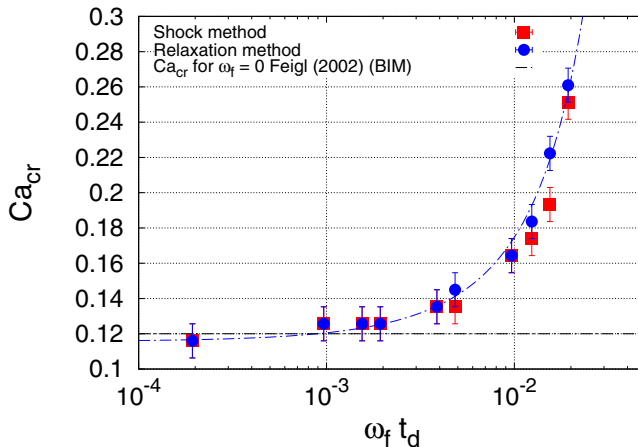
FIG. 8. Critical capillary number Ca_{cr} against different frequencies $\omega_f t_d$ for a droplet in an unconfined elongational flow. We consider the two breakup protocols, the *shock method* and the *relaxation method*. Even though the droplet breakup is dependent on the shear rate frequency $\omega_f t_d$, a protocol mismatch does not occur, contrary to the case of the confined shear flow topology. The error bars are estimated via steps in the critical capillary number ΔCa.

VIII. CONCLUSIONS AND OUTLOOK

We have shown that the interplay of varying startup conditions and strong confinement ratios can lead to qualitatively and quantitatively different droplet breakup conditions in stationary shear flows, unlike the stable equilibria found for varying startup conditions [57] or the ones found for varying degrees of confinement [14]. Having investigated the effects of inertia, confinement and flow topology, we conclude that the protocol mismatch between the shock and the relaxation method are due to a high degree of confinement for a droplet in a shear flow ($\alpha = 0.75$). However, the breakup solution found via the relaxation method is only metastable, since it becomes unstable in the case of a time-dependent, oscillatory shear flow. The protocol mismatch is thus solely due to an extra metastable solution in a strongly confined shear flow and disappears in the presence of small perturbations (e.g., amplitude variations in an oscillatory shear flow) in accordance with the uniqueness of the Stokes solution [14,57]. We have also shown the dependency of the critical capillary number Ca_{cr} on the normalized oscillation frequency $\omega_f t_d$ in both oscillatory shear and elongational flows. In the case of the elongational flow, Ca_{cr} increases with increasing $\omega_f t_d$, whereas no simple functional dependence can be found for the oscillatory shear flow, since Ca_{cr} also depends on the flow startup and degree of confinement. We should stress again that the results presented in this work are only valid for $\chi = 1$, since the viscosity ratio influences the breakup of a confined droplet [8,14,21,22]. On the one hand, for small viscosity ratios $\chi \approx 0.3$ the confined shear flow stabilises the droplet and breakup is more difficult to occur than for $\chi = 1$. On the other hand for large viscosity ratios $\chi \approx 5.0$ the confined droplet is destabilized and breakup is more likely to happen than for $\chi = 1$ [14,21]. It would be interesting to see whether the metastable solution can be found in an experimental setup or whether it is too prone to perturbations to manifests itself.

[1] R. W. Flumerfelt, Drop breakup in simple shear fields of viscoleastic fluids, Ind. Eng. Chem. Fundam. **11**, 312 (1972).

[2] J. Rodriguez-Rodriguez, A. Sevilla, C. Martinez-Bazan, and J. M. Gordillo, Generation of microbubbles with applications to industry and medicine, Annu. Rev. Fluid Mech. **47**, 405 (2015).

[3] H. Shewan and J. R. Stokes, Review of techniques to manufacture microhydrogel particles for the food industry and their applications, J. Food Eng. **119**, 781 (2013).

[4] M. Singh, H. M. Haverinen, and P. Dhagat, Inkjet printing-process and its applications, Adv. Funct. Mater. **22**, 673 (2010).

[5] I. Fortelny and J. Juza, Description of the droplet size evolution in flowing immiscible polymer blends, Polymers **11**, 761 (2019).

[6] F. Greco, Drop deformation for non-Newtonian fluids in slow flows, J. Non-Newtonian Fluid Mech. **107**, 111 (2002).

[7] Stefano Guido and Francesco Greco, Dynamics of a liquid drop in a flowing immiscible liquid, Rheol. Rev. **2**, 99 (2004).

[8] P. J. A. Janssen and P. D. Anderson, A boundary-integral model for drop deformation between two parallel plates with nonunit viscosity ratio drops, J. Comput. Phys. **227**, 8807 (2008).

[9] G. I. Taylor, The viscosity of a fluid containing small drops of another fluid, Proc. Roy. Soc. A: Math. Phys. Eng. Sci. **138**, 41 (1932).

[10] F. Greco, Second-order theory for the deformation of a Newtonian drop in a stationary flow field, Phys. Fluids (1994-present) **14**, 946 (2002).

[11] A. Acrivos and T. D. Taylor, The Stokes flow past an arbitrary particle, Chem. Eng. Sci. **19**, 445 (1964).

[12] J. Lyngaae-Jørgensen and A. Valenza, Structuring of polymer blends in simple shear flow, Makromol. Chem. Macromol. Symp. **38**, 43 (1990).

[13] S. Guido, Shear-induced droplet deformation: Effects of confined geometry and viscoelasticity, Curr. Opin. Colloid Interface Sci. **16**, 61 (2011).

[14] P. J. A. Janssen, A. Vananroye, P. Van Puyvelde, P. Moldenaers, and P. D. Anderson, Generalized behavior of the breakup of viscous drops in confinements, J. Rheol. **54**, 1047 (2010).

[15] A. Vananroye, R. Cardinaels, P. Van Puyvelde, and P. Moldenaers, Effect of confinement and viscosity ratio on the dynamics of single droplets during transient shear flow, J. Rheol. **52**, 1459 (2008).

[16] R. Cardinaels and P. Moldenaers, Droplet relaxation in blends with one viscoelastic component: Bulk and confined conditions, Rheologica Acta **49**, 941 (2010).

[17] R. Cardinaels and P. Moldenaers, Critical conditions and breakup of nonsquashed microconfined droplets: Effects of fluid viscoelasticity, Microfluid Nanofluid **10**, 1153 (2011).

[18] R. Cardinaels, K. Verhulst, and P. Moldenaers, Influence of confinement on the steady state behavior of single droplets in shear flow for immiscible blends with one viscoelastic component, J. Rheol. (1978-present) **53**, 1403 (2009).

[19] R. Cardinaels, A. Vananroye, P. Van Puyvelde, and P. Moldenaers, Breakup criteria for confined droplets: Effects of compatibilization and component viscoelasticity, Macromol. Mater. Eng. **296**, 214 (2011).

[20] P. De Bruyn, R. Cardinaels, and P. Moldenaers, The effect of geometrical confinement on coalescence efficiency of droplet pairs in shear flow, J. Colloid Interface Sci. **409**, 183 (2013).

[21] P. Van Puyvelde, A. Vananroye, R. Cardinaels, and P. Moldenaers, Review on morphology development of immiscible blends in confined shear flow, Polymer **49**, 5363 (2008).

[22] A. Vananroye, P. Van Puyvelde, and P. Moldenaers, Effect of confinement on droplet breakup in sheared emulsions, Langmuir **22**, 3972 (2006).

[23] A. Vananroye, P. Van Puyvelde, and P. Moldenaers, Effect of confinement on the steady-state behavior of single droplets during shear flow, J. Rheol. **51**, 139 (2007).

[24] A. Vananroye, P. Van Puyvelde, and P. Moldenaers, Deformation and orientation of single droplets during shear flow: Combined effects of confinement and compatibilization, Rheologica acta **50**, 231 (2011).

[25] M. Shapira and S. Haber, Low reynolds number motion of a droplet between two parallel plates, Int. J. Multiph. Flow **14**, 483 (1988).

[26] M. Shapira and S. Haber, Low reynolds-number motion of a droplet in shear flow including wall effects, Int. J. Multiph. Flow **16**, 305 (1990).

[27] G. I. Taylor, The formation of emulsion in definable field of flow, Proc. Roy. Soc. A **146**, 501 (1934).

[28] P. L. Maffettone and M. Minale, Equation of change for ellipsoidal drops in viscous flow, J. Non-Newton. Fluid Mech **78**, 227 (1998).

[29] M. Minale, A phenomenological model for wall effects on the deformation of an ellipsoidal drop in viscous flow, Rheol. Acta **47**, 667 (2008).

[30] M. Minale, Models for the deformation of a single ellipsoidal drop: A review, Rheol. Acta **49**, 789 (2010).

[31] V. Sibillo, G. Pasquariello, M. Simeone, V. Cristini, and S. Guido, Drop Deformation in Microconfined Shear Flow, Phys. Rev. Lett. **97**, 054502 (2006).

[32] M. Minale, S. Caserta, and S. Guido, Microconfined shear deformation of a droplet in an equiviscous non-Newtonian immiscible fluid: Experiments and modeling, Langmuir **26**, 126 (2010).

[33] N. Aggarwal and K. Sarkar, Deformation and breakup of a viscoelastic drop in a Newtonian matrix under steady shear, J. Fluid Mech. **584**, 1 (2007).

[34] N. Aggarwal and K. Sarkar, Effects of matrix viscoelasticity on viscous and viscoelastic drop deformation in a shear flow, J. Fluid Mech. **601**, 63 (2008).

[35] S. Caserta, S. Reynaud, M. Simeone, and S. Guido, Drop deformation in sheared polymer blends, J. Rheol. **51**, 761 (2007).

[36] C. E. Chaffey and H. A. Brenner, A second-order theory for shear deformation of drops, J. Colloid Interface Sci. **24**, 258 (1967).

[37] T. Chinyoka, Y. Y. Renardy, M. Renardy, and D. B. Khismatullin, Two-dimensional study of drop deformation under simple shear for Oldroyd-B liquids, J. Non-Newtonian Fluid Mech. **130**, 45 (2005).

[38] J. J. Elmendorp and R. J. Maalcke, A study on polymer blending microrheology: Part 1, Polym. Eng. Sci. **25**, 1041 (1985).

[39] K. Feigl, S. F. M. Kaufmann, P. Fischer, and E. J. Windhab, A numerical procedure for calculating droplet deformation in dispersing flows and experimental verification, Chem. Eng. Sci. **58**, 2351 (2002).

[40] H. P. Grace, Dispersion phenomena in high viscosity immiscible fluid systems and application of static mixers as dispersion devices in such systems, Chem. Eng. Commun. **14**, 225 (1982).

[41] A. E. Komrakovaa, O. Shardt, D. Eskinb, and J. J. Derksen, Lattice Boltzmann simulations of drop deformation and breakup in shear flow, Int. J. Multiphase Flow **59**, 24 (2014).

[42] H. Li and U. Sundararaj, Does drop size affect the mechanism of viscoelastic drop breakup? Phys. Fluids **20**, 053101 (2008).

[43] J. Li, Y. Y. Renardy, and M. Renardy, Numerical simulation of breakup of a viscous drop in simple shear flow through a volume-of-fluid method, Phys. Fluids **12**, 269 (2000).

[44] H. Liu, A. J. Valocchi, and Q. Kang, Three-dimensional lattice Boltzmann model for immiscible two-phase flow simulations, Phys. Rev. E **85**, 046309 (2012).

[45] D. Megias-Alguacil, K. Feigl, M. Dressler, P. Fischer, and E. J. Windhab, Droplet deformation under simple shear investigated by experiment, numerical simulation and modeling, J. Non-Newtonian Fluid Mech. **126**, 153 (2005).

[46] F. Mighri and M. A. Huneault, In situ visualization of drop deformation, erosion, and breakup in high viscosity ratio polymeric systems under high shearing stress conditions, J. Appl. Polym. Sci. **42**, 25822591 (2006).

[47] F. Mighri, P. J. Carreau, and A. Ajji, Influence of elastic properties on drop deformation and breakup in shear flow, J. Rheol. (1978-present) **42**, 1477 (1998).

[48] S. Mukherjee and K. Sarkar, Effects of viscosity ratio on deformation of a viscoelastic drop in a Newtonian matrix under steady shear, J. Non-Newtonian Fluid Mech. **160**, 104 (2009).

[49] S. B. Pillapakkam and P. Singh, A level-set method for computing solutions to viscoelastic two-phase flow, J. Comput. Phys. **174**, 552 (2001).

[50] Y. Y. Renardy and V. Cristini, Effect of inertia on drop breakup under shear, Phys. Fluids **13**, 7 (2001).

[51] V. Sibillo, M. Simeone, and S. Guido, Breakup of a Newtonian drop in a viscoelastic matrix under simple shear flow, Rheol. Acta **43**, 449 (2004).

[52] C. L. Tucker and P. Moldenaers, Microstructural evolution in polymer blends, Annu. Rev. Fluid Mech. **34**, 177 (2002).

[53] X. Zhao, Drop breakup in dilute Newtonian emulsions in simple shear flow: New drop breakup mechanisms, J. Rheol. **51**, 367 (2007).

[54] B. J. Bentley and L. G. Leal, An experimental investigation of drop deformation and breakup in steady two-dimensional linear flows, J. Fluid Mech. **167**, 241 (1986).

[55] J. F. Brady and A. Acrivos, The deformation and breakup of a slender drop in an extensional flow: Inertial effects, J. Fluid Mech. **115**, 443 (1982).

[56] E. J. Hinch and A. Acrivos, Long slender drops in a simple shear flow, J. Fluid Mech. **98**, 305 (1980).

[57] Y. Renardy, Effect of startup conditions on drop breakup under shear with inertia, J. Multiphase Flow **34**, 1185 (2008).

[58] S. Torza, R. G. Cox, and S. G. Mason, Particle motions in sheared suspensions XXVII. Transient and steady deformation and burst of liquid drops, J. Colloid Interface Sci. **38**, 395 (1972).

[59] R. Cavallo, S. Guido, and M. Simeone, Drop deformation under small-amplitude oscillatory shear flow, Rheol Acta **42**, 1 (2002).

[60] R. G. Cox, The deformation of a drop in a general time-dependent fluid flow, J. Fluid Mech. **37**, 601 (1969).

[61] A. Farutin and C. Misbah, Rheology of vesicle suspensions under combined steady and oscillating shear flows, J. Fluid Mech. **700**, 362 (2012).

[62] F. Milan, M. Sbragaglia, L. Biferale, and F. Toschi, Lattice Boltzmann simulations of droplet dynamics in time-dependent flows, Eur. Phys. J. E **41**, 6 (2018).

[63] W. Yu., M. Bousmina, M. Grmela, and C. Zhou, Modeling of oscillatory shear flow of emulsions under small and large deformation fields, J. Rheol. **46**, 1401 (2002).

[64] R. Benzi, S. Succi, and M. Vergassola, The lattice Boltzmann equation: Theory and applications, Phys. Rep. **222**, 145 (1992).

[65] S. Succi, *The Lattice Boltzmann Equation for Fluid Dynamics and Beyond* (Oxford University Press, Oxford, UK, 2001).

[66] M. Sbragaglia, R. Benzi, M. Bernaschi, and S. Succi, The emergence of supramolecular forces from lattice kinetic models of nonideal fluids: Applications to the rheology of soft glassy materials, Soft Matter **8**, 10773 (2012).

[67] J. Onishi, Y. Chen, and H. Ohashi, A lattice Boltzmann model for polymeric liquids, Prog. Comp. Fluid Dyn. **5**, 75 (2005).

[68] M. Gross, M. E. Cates, F. Varnik, and R. Adhikari, Langevin theory of fluctuations in the discrete Boltzmann equation, J. Stat. Mech. (2011) P03030.

[69] X. Xue, M. Sbragaglia, L. Biferale, and F. Toschi, Effects of thermal fluctuations in the fragmentation of a nanoligament, Phys. Rev. E **98**, 012802 (2018).

[70] D. Chiappini, X. Xue, G. Falcucci, and M. Sbragaglia, Ligament breakup simulation through pseudopotential lattice Boltzmann method, In *AIP Conference Proceedings*, Vol. 1978 (AIP Publishing, 2018), p. 420003.

[71] D. Chiappini, M. Sbragaglia, X. Xue, and G. Falcucci, Hydrodynamic behavior of the pseudopotential lattice Boltzmann method for interfacial flows, Phys. Rev. E **99**, 053305 (2019).

[72] S. Farokhirad, T. Lee, and J. F. Morris, Effects of inertia and viscosity on single droplet deformation in confined shear flow, Commun. Comput. Phys. **13**, 706 (2013).

[73] A. Gupta and M. Sbragaglia, Deformation and breakup of viscoelastic droplets in confined shear flow, Phys. Rev. E: Stat. Nonlin. Soft Matter Phys. **90**, 1 (2014).

[74] A. Gupta, M. Sbragaglia, and A. Scagliarini, Hybrid lattice Boltzmann/finite difference simulations of viscoelastic multicomponent flows in confined geometries, J. Comput. Phys. **291**, 177 (2015).

[75] J. Onishi, Y. Chen, and H. Ohashi, Dynamic simulation of multicomponent viscoelastic fluids using the lattice Boltzmann method, Physica A **362**, 84 (2006).

[76] H. Xi and C. Duncan, Lattice Boltzmann simulations of three-dimensional single droplet deformation and breakup under simple shear flow, Phys. Rev. E **59**, 3022 (1999).

[77] M. Yoshino, Y. Toriumi, and M. Arai, Lattice Boltzmann simulation of two-phase viscoelastic fluid flows, J. Comput. Sci. Technol. **2**, 330 (2008).

[78] X. Shan and H. Chen, Lattice Boltzmann model for simulating flows with multiple phases and components, Phys. Rev. E **47**, 1815 (1993).

[79] X. Shan and H. Chen, Simulation of nonideal gases and liquid-gas phase transitions by the lattice Boltzmann equation, Phys. Rev. E **49**, 2941 (1994).

[80] M. Sbragaglia and D. Belardinellli, Interaction pressure tensor for a class of multicomponent lattice Boltzmann models, Phys. Rev. E **88**, 013306 (2013).

[81] M. Sega, M. Sbragaglia, S. Kantorovich, and A. Ivanov, Interaction pressure tensor for a class of multicomponent lattice Boltzmann models, Soft Matter **9**, 10092 (2013).

[82] D. d'Humières, I. Ginzburg, M. Krafczyk, P. Lallemand, and L. Luo, Multiple-relaxation-time lattice Boltzmann models in three dimensions, Roy. Soc. **360**, 437 (2002).

[83] M. Hecht and J. Harting, Implementation of on-site velocity boundary conditions for d3q19 lattice Boltzmann simulations, J. Stat. Mech. (2010) P01018.

[84] K. Mattila, J. Hyväluoma, and T. Rossi, Mass-flux-based outlet boundary conditions for the lattice Boltzmann method, J. Stat. Mech. (2009) P06015.

[85] Q. Zou and X. He, On pressure and velocity boundary conditions for the lattice Boltzmann BGK model, Phys. Fluids **9**, 1591 (1997).

[86] L. Biferale, P. Perlekar, M. Sbragaglia, S. Srivastava, and F. Toschi, A lattice Boltzmann method for turbulent emulsions, J. Phys.: Conf. Ser. **318**, 052017 (2011).